Resistance schemes in shallow overland flow along a hillslope covered with patchy vegetation

Octavia Crompton [1,2] Gabriel G. Katul [3] Sally Thompson [2,4]

[1]Department of Earth and Planetary Sciences, University of California, Berkeley, CA, USA.
[2]Department of Civil and Environmental Engineering, University of California, Berkeley, CA, USA.
[3]Nicholas School of the Environment, Duke University, Durham, NC, USA
[4]Department of Environmental Engineering, University of Western Australia, Perth, WA, Australia.

Key Points:

- Roughness effects in non-kinematic overland flow can be approximated using a kinematic wave approximation
- The sensitivity of hydrological predictions to the depth-velocity scaling exponents closing the friction slope is small
- Parameterizing the 'scale' of roughness remains a key source of uncertainty

Corresponding author: Octavia Crompton, `octavia@berkeley.edu`

Abstract

Parameterizing the effects of surface roughness on flow resistance remains a major challenge in modeling overland flow using physics-based descriptions such as the Saint Venant equations (SVE). This challenge has prompted the development of a large number of roughness schemes relating the properties of a rough surface, the bulk velocity and resistance, yet it is often unclear which of these schemes should be used to represent a given land surface, particularly on heterogeneous surfaces. Since it is often necessary to calibrate any given roughness scheme to flow on a given surface, modelers need to understand the sensitivity of their predictions to the choice of roughness scheme, post calibration. Here, we focus on hillslope-scale predictions made with the SVE: the water balance partitioning between runoff and infiltration, the hillslope hydrograph, and the discharge velocity. We develop an approach to calibrate roughness schemes to each other, by undertaking the calibration under equilibrium flow conditions and imposing the kinematic wave approximation at the outlet. This approach yields analytical relationships between the parameters of two roughness schemes applied to the same hillslope and discharge. We apply this approach to a sensitivity analysis of hydrological predictions resulting from the choice of five commonly used roughness schemes. The results suggest that, once calibrated, there is minimal prediction sensitivity to the choice of scheme across a wide range of rainfall conditions. Operationally, these results mean that the parameterization of any selected roughness scheme is more important for predicting the hydrological behavior than the selection of a particular scheme.

1 Introduction

Overland flow is ubiquitous in locations with low soil permeability, such as mountainous, arid, urban or agricultural landscapes (Descroix, Viramontes, Estrada, Barrios, & Asseline, 2007; Dunne, 1983; Li, Sivapalan, Tian, & Harman, 2014). Overland flow occurs at the expense of infiltration and is responsible for soil erosion and flash flooding (Abrahams, Parsons, & Wainwright, 1994; Bracken, Cox, & Shannon, 2008). The occurrence, depth, velocity, and time evolution of overland flow during and after storms is therefore relevant to land managers, practitioners, scientists, and engineers (Cantón et al., 2011; Hallema, Moussa, Sun, & McNulty, 2016). In dryland environments, overland flow occurs on patchily-vegetated landscapes with spatially varying infiltration properties, roughness and slopes.

The most general physical equations with which to represent flow in such environments are the Saint Venant (or shallow water) equations (SVE). These equations combine the continuity equation with the conservation of momentum, and are shown here in their one-dimensional form for illustration:

$$\frac{\partial h}{\partial t} + \frac{\partial}{\partial x}(Uh) = p - i, \tag{1}$$

$$\frac{\partial U}{\partial t} + U\frac{\partial U}{\partial x} + g\frac{\partial h}{\partial x} + g(S_f - S_o) + \frac{U(p-i)}{h} = 0, \tag{2}$$

where h is the water depth at location x and time t, U is the depth-averaged velocity, S_o and S_f are the bed- and friction- slopes, and g is the gravitational acceleration. The boundary conditions are rainfall p and infiltration losses i that can vary with x and t.

The SVE do not form a closed system of equations, and users must specify a closure model for the friction slope S_f, which represents the net effects of bed and other shear stresses (e.g. presence of obstructions) on the flow. The closure model takes the form of a resistance formulation (colloquially, a 'roughness scheme') that describes S_f in terms of the modeled flow variables (i.e. h and U), subject to constraints based on the genesis of frictional resistance to flow. Roughness schemes must be defined even if the full SVE is simplified to the dynamic or kinematic wave equations.

Resistance formulations for overland flow capture the effects of two sources of friction: (i) friction imposed by shear created when the flow traverses the land surface (known as bed friction) and (ii) friction produced when solid bodies such as soil, rocks, vegetation stems and leaves obstruct or protrude into the flow. Because these solid bodies may be present across some or all of the water column, they are often referred to as distributed roughness elements. Early work in hydraulics developed numerous resistance formulations to describe bed shear stresses (Gauckler, 1867; Manning, Griffith, Pigot, & Vernon-Harcourt, 1890), which have been elaborated on and extended to distributed roughness elements by subsequent studies of the flow boundary layer (e.g. Brutsaert, 2005; Cheng & Nguyen, 2010; Katul, Poggi, & Ridolfi, 2011; Kirstetter et al., 2016; Mügler et al., 2011; Wang, Huai, Thompson, & Katul, 2015). A subset of these schemes is summarized in Table 1, and their derivation is reviewed in supporting information Text S1. Note that these schemes are presented in their one-dimensional form for simplicity, but implemented in two-dimensions in the model presented here.

Despite the differing sources of friction addressed by the roughness schemes, the forms of the resistance equations in Table 1 share a number of common features. For example, all of the equations can be represented as a dimensionless Froude number ($Fr^2 \sim \frac{U^2}{ghS_f}$) that depends either on the roughness properties of the surface, the bulk or elemental Reynolds number ($Re \sim Uh/\nu$, where ν is the kinematic viscosity, and where h can be replaced by an element-based lengthscale where appropriate), or both (see supporting information Text S1). As such, these resistance schemes are inherently power-law expressions linking U to h via an exponent and a scaling coefficient, whose function, loosely, is to set the magnitude of frictional resistance (such as n in Manning's equation). The exponents are independent of any calibration, and their impacts on resistance vary between roughness schemes. Even after the scaling parameters are calibrated, different roughness schemes may result in different predictions because their exponents differ.

The purpose of this technical note is to quantify the consequences of selecting different roughness schemes for flow prediction on a synthetic dryland hillslope, in which vegetation cover is generally patchy but can vary from uniformly absent to completely vegetated. Such a hillslope provides an example of a landscape on which the 'best' choice of roughness scheme is ambiguous. This ambiguity arises from the sparse, patchy distribution of vegetation, and the shallow but disturbed nature of the flow. We address two questions:

(i) How can different roughness schemes be simply calibrated against each other on biphasic, heterogeneous landscapes, to facilitate inter-comparison of predictions? and
(ii) Following such calibration, how sensitive are the hydrological predictions made on these landscapes to the selection of a roughness scheme?

Answering these basic methodological questions offers guidance regarding the likely sensitivity of predictions to the choice of roughness scheme.

2 Methods

2.1 A framework for cross-comparison

[c1]Despite the common non-dimensional scaling that lies behind the roughness schemes (see supporting information Text S1), the derived resistance equations embed distinct ways to conceptualize a rough surface, and distinct parameterizations of the

[c1] *Text added.*

Table 1. Summary of the relations between the dimensionless Froude number $Fr^2 = U^2/gS_fh$ and friction factor f, as well as the resulting conveyance equation, where α is a general resistance parameter. To compare to the published forms, $S_f = S_o$, which is the kinematic wave approximation to the momentum balance (Equation 2) in the SVE.

Name	Resistance equation	Conveyance equation	References
Bed resistance equations			
Darcy-Weisbach	$Fr^2 = \frac{8}{f}$	$U = \frac{1}{\alpha} h^{1/2} S_o^{1/2}$	Brutsaert (2005)
		$\alpha = \sqrt{\frac{f}{8g}}$	Cea, Legout, Darboux, Esteves, and Nord (2014)
Poisseuille	$Fr^2 = \frac{Uh}{3\nu}$	$U = \frac{1}{\alpha} h^2 S_o$	Brutsaert (2005)
		$\alpha = \frac{3\nu}{g}$	Kirstetter et al. (2016)
Manning	$Fr^2 = \frac{h^{1/3}}{n^2 g}$	$U = \frac{1}{\alpha} h^{2/3} S_o^{1/2}$	Brutsaert (2005)
		$\alpha = n$	Smith, Cox, and Bracken (2007)
Transitional /	$Fr^2 = \frac{8}{a\epsilon}$	$U = \frac{1}{\alpha} h S_o^{1/2}$	Brutsaert (2005)
Mixed-flow		$\alpha = \frac{a\epsilon}{8g}$	Horton (1938)
Distributed drag equations			
Cylinder array	$Fr^2 = \frac{2(1-\phi)}{C_d \mu D h}$	$U = \frac{1}{\alpha}\sqrt{S_o}$	Cheng and Nguyen (2010)
		$\alpha = \sqrt{\frac{C_d \mu D}{2g(1-\phi)}}$	Tanino and Nepf (2008)
Poggi	$Fr^2 = \frac{1}{\beta^2} \exp\left(\frac{-H_c}{\beta^2 L_c}\right)$	$U = \frac{1}{\alpha} h^{1/2} S_o^{1/2}$	Katul et al. (2011)
		$\alpha = \frac{\sqrt{\beta}}{g} \exp\left(\frac{H_c}{2\beta^2 L_c}\right)$	
Depth-dependent Manning	$Fr^2 = \frac{h}{n_o^2 g h_o^{2/3}}$	$U = \frac{1}{\alpha} h S_o^{1/2}$	Mügler et al. (2011)
		$\alpha = n_o h_o^{1/3}$	Jain, Kothyari, and Raju (2004)

surface features. In order to ask whether predictions are sensitive to the choice of a scheme, the predictions made using different schemes need to be placed within a common framework to enable cross-comparison. Here, we develop such a framework via an analytical calibration procedure.

Cross-comparison of schemes is facilitated by the similarities in their mathematical form when expressed in terms of the kinematic conveyance equation (the third column in Table 1) relating the flow velocity to the flow depth, the bed slope, and a range of other parameters, which can be lumped together as a single factor α (Brutsaert, 2005; Lighthill & Whitham, 1955).

$$U = \frac{1}{\alpha} h^m S_o^\eta. \tag{3}$$

where α and m are generalized coefficients describing the surface roughness and flow regime, respectively, discussed in greater detail below.

The units and physical interpretation of α are scheme-specific, but in general, α increases with increasing surface roughness. The flow regime (laminar, transitional, turbulent), which sets the value of b in the generalized $f \sim a\epsilon^b$ expression, emerges in Equation 3 as m. Figure 1 illustrates how surface roughness α and flow regime m affect the relation between U and h for a fixed hillslope gradient, S_o.

To compare predictions made by the schemes, the values of α used in each scheme must be chosen to minimize the differences in their predictions for a common situation. If one scheme is treated as a reference, then this selection problem is essentially one of calibration. To enable the use of an analytical framework, we assume that the conveyance equation above applies at hillslope scales, even on the potentially complex hillslopes considered later. With this assumption, the calibration problem admits analytical solutions for homogeneous hillslopes, if flow conditions are calibrated to each other at the hillslope outlet (as outlined in Section 2.2). We then consider how this method can be adapted to patchily vegetated slopes, assuming that there is a known resistance equation that applies to bare sites on those slopes. We outline this method in Section 2.3. With the α values selected to minimize disagreement between schemes, remaining differences in flow predictions can be attributed to the unique physics implied by each resistance scheme, which alters the relationship between flow velocity and depth (for example, the distinctions seen between the curves in Figure 1 panel A).

[c5]We use a coupled Saint Venant - Richards equation model to evaluate the differences in predicted hillslope-scale hydrology associated with different roughness schemes [c6] [c7]following calibration of their roughness coefficients to each other (Section 2.4). We undertake this evaluation for a wide and realistic range of storm and hillslope scenarios.

2.2 Calibration strategy for homogeneous slopes

We start with the problem of determining a roughness parameterization that will relate two different roughness schemes for the same rain intensity on a common slope. To proceed to an analytical solution, we consider the idealized situation of a hillslope exposed to constant rainfall p on which infiltration occurs at a constant rate given by the hydraulic conductivity K_s.

[c5] *OC*: ~~A coupled Saint Venant - Richards equation model is then used~~
[c6] *ST*: ~~after their~~
[c7] *OC*: ~~kinematic conveyance equations have been calibrated to reference flow conditions~~

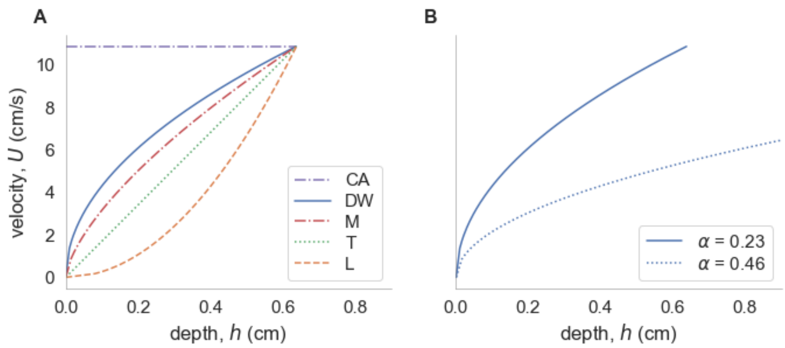

Figure 1. Illustration of the independent roles of the selection of a roughness scheme (m) and its parameterization (α) on the predicted kinematic relation between velocity and depth. [c3] (A) illustrates how the selection of a roughness scheme implies a $U - h$ scaling relation for each roughness scheme, independent of the value of α (for each scheme, α has been calibrated to preserve flow properties between schemes at the outlet, as described in Section 2.2). [c4] Conversely, (B) shows Darcy Weisbach flow on landscapes with two different values of α.

Under steady-state conditions, the kinematic conveyance equations in Table 1 specify the relationships between discharge, velocity and stage. Additionally, at the hillslope outlet, discharge must be balanced by hillslope-scale rainfall inputs, such that on a per-unit-hillslope width basis:

$$q_o = Uh = L(p - K_s), \tag{4}$$

where L is the hillslope length and q_o is the flow rate at the outlet per unit width. We now consider that two different conveyance equations could be used to describe this flow:

$$U_1 = \frac{1}{\alpha_1} h_1^{m_1} S_o^{\eta_1} \tag{5}$$

$$U_2 = \frac{1}{\alpha_2} h_2^{m_2} S_o^{\eta_2} \tag{6}$$

Given that our interest is in representing hillslope-scale hydrological responses (which are evaluated at the hillslope outlet), we specify that the flow variables at the outlet should be conserved between the schemes, such that $U_1 = U_2$ and $h_1 = h_2$ at the outflow point.

Firstly, an expression for the flow depth at the outlet in the first scheme can be written as a function of the hillslope discharge q_o:

$$h_1 = \frac{q_o}{U_1} \tag{7}$$

$$= q_o \alpha_1 S_o^{-\eta_1} h_1^{-m_1}. \tag{8}$$

Rearranging:

$$h_1 = (\alpha_1 q_o S_o^{-\eta_1})^{1/(m_1+1)}. \tag{9}$$

Substituting Equation 9 into Equation 5:

$$U_1 = \frac{1}{\alpha_1} S_o^{\eta_1} (\alpha_1 q_o S_o^{-\eta_1})^{m_1/(m_1+1)}, \tag{10}$$

which simplifies to:

$$U_1 = \left(\frac{S_o^{\eta_1} q_o^{m_1}}{\alpha_1} \right)^{1/(m_1+1)}. \tag{11}$$

Because α_1 is known, U_1 in Equation 11 is also known. The same logic means that the outlet velocity U_2 in the second roughness scheme can be written in the same form, and rearranged to isolate the roughness term α_2:

$$\alpha_2 = \frac{S_o^{\eta_2} q_o^{m_2}}{U_2^{m_2+1}}. \tag{12}$$

At this point, we require the outlet velocities to be equal between the two schemes, and combine Equations 11 and 12 to obtain an analytic expression for α_2 in terms of the scaling exponents of the roughness expressions (i.e. m_1 and m_2), the equilibrium discharge q_o, and the roughness parameter of the first scheme α_1:

$$\alpha_2 = \left[\alpha_1^{m_2+1} S_o^{\eta_2(m_1+1)-\eta_1(m_2+1)} q_o^{m_2-m_1}\right]^{1/(m_1+1)}. \tag{13}$$

[c1]

This approach effectively calibrates the two schemes to each other at the outlet, for a given hillslope and rainfall rate. The calibration quantifies an α_2 that produces equivalent flow at the outlet to the reference scheme with α_1, for a given set of storm and landscape parameters. The same result is obtained if the derivation proceeds by requiring $h_1 = h_2$ at the outlet, as expected given the constraint that q_o is the same for both schemes.

The dependence of Equation 13 on slope length and rainfall rate (via q_o) [c2] [c3]reflects the fact that the calibrated α_2 absorbs differences in prediction that arise from differences in m and η between the schemes, and thus depends on the h and U associated with equilibrium flow. The calibrated α_2 is therefore not an independent description of the surface roughness, but rather, a parameterization that is adjusted for the magnitude of the flow and the differences in resistance that emerge between roughness schemes for that flow.

Because the schemes are forced to agree at the outlet, differences in predicted U and h values will emerge at other locations on the hillslope. Thus, this calibration approach is appropriate for evaluating differences in hillslope-average flow properties after adjusting the roughness parameters [c4](α) to minimize those differences under equilibrium flow conditions. Differences between schemes during unsteady conditions or at other locations on the hillslope are not minimized by this approach. [c5] However, the analytic tractability of the approach renders it attractive, as it requires no additional model runs to calibrate α_2. An alternative calibration approach would be to conduct multiple model runs to achieve near-exact agreement over one assessment metric (e.g. infiltration fraction), and assess the quality of the match over a different set of assessment metrics (e.g. hydrograph NRMSE, t_{rise} and U_{max}); however, such an approach would require multiple model runs for storm and hillslope case, which would be computationally more demanding and lacks theoretical underpinning.

[c1] *OC*: ~~The same result is obtained if the derivation proceeds by requiring $h_1 = h_2$ at the outlet, as expected given the constraint that q_o is the same for both schemes.~~

[c2] *ST*: ~~implicitly accounts for~~

[c3] *ST*: *Text added.*

[c4] *OC*: *Text added.*

[c5] *OC*: ~~However, the analytic tractability of the approach renders it attractive relative to other optimization approaches for α_2 that would require multiple model runs.~~

2.3 Calibration strategy for patchy hillslopes

We now extend the calibration strategy from homogeneous hillslopes (described in the previous section), to patchy landscapes, addressing the additional complexity of flow processes on these landscapes. To simplify the process, we consider a hillslope that can be represented as a binary mosaic of vegetated and bare soil areas [c6]<u>(see Figure 2)</u>. Infiltration rates are assumed to be low in bare areas due to the formation of surface crusts (Assouline, 2004; Assouline et al., 2015) and higher under vegetation cover due to root activity and protection of the soil surface against rain-splash by the canopy (Thompson, Harman, Heine, & Katul, 2010). Roughness characteristics are similarly determined by whether the surface is bare or vegetated. To further simplify the approach, we assume that the bare sites are impermeable and have known roughness. [c7]<u>The spatial pattern of bare and vegetated sites is described by the vegetation cover fraction ϕ_V and a characteristic length-scale σ describing the spatial correlation of the patches (see supporting information Figure S1 for a summary of the methods used to generate the vegetation patterns).</u>

While the impermeable bare soil areas are always sources of runoff, the vegetated patches may function as runoff sources or sinks, depending on the values of p and K_s. This requires adjustment to the calibration approach, [c1]<u>which is achieved</u> by separately considering 3 cases: p greater than, approximately equal to, and less than K_s. [c2]<u>Because the heterogeneous land surfaces are two-dimensional, the calibration approach uses a one-dimensional approximation, with the vegetation fields summarized by one-dimensional statistics (e.g. vegetation fraction and characteristic patch length).</u> Lastly, interception losses by the vegetation have been ignored here but could be readily accommodated by adjusting p.

2.3.1 Case 1: Rainfall intensity greater than hydraulic conductivity

In this case, the entire hillslope is a runoff source. Vegetated patches generate runoff at the rate $p - K_s$, and bare soil areas generate runoff at the rate p. For the purpose of predicting hillslope-average outcomes, we can treat the hillslope as a homogeneous surface, provided that we adjust the discharge at the outlet q_o to account for the different surface types. To do this, we approximate q_o as:

$$q_o = L[p(1 - \phi_V) + (p - K_s)\phi_V], \tag{14}$$

and Equation 13 is otherwise unchanged.

2.3.2 Case 2: Rainfall intensity less than hydraulic conductivity

In this situation, runoff is generated on the bare soil patches, but the vegetated patches act as sinks into which some or all of the runoff infiltrates. The effect of the vegetated areas acting as sinks is that the fraction of the hillslope generating runoff is reduced to a maximum of $1-\phi_V$. In the most extreme case, only the patches that are immediately adjacent to the hillslope outlet generate runoff (the so-called ‘directly connected areas’ (Alley & Veenhuis, 1983; Booth & Jackson, 1997; Lee & Heaney, 2003; Leopold, 1968)).

[c6] *OC*: *Text added.*

[c7] *OC*: ~~The proportion of bare and vegetated sites is described by the vegetation cover fraction ϕ_V and the characteristic length-scale of the bare patches, L_B, describing the spatial correlation of the patches.~~

[c1] *OC*: ~~which we approach~~

[c2] *OC*: ~~Although the heterogeneous land surface is two-dimensional, the calibration approach uses a one-dimensional approximation.~~

To account for this, we consider the behavior of runoff generated by an individual representative bare soil patch. We apply the calibration approach at the bottom boundary of this patch. Thus, q_o in Equation 13 is replaced with:

$$q_o = L_b p. \tag{15}$$

where L_b is the mean along-slope length of the bare soil areas.

2.3.3 Case 3: Rainfall intensity equal to hydraulic conductivity

For the situation where $p = K_s$, either patch or hillslope-scale calibration approaches could be used. Patch-scale calibration would be expected to produce better results for outcomes related to runoff generation from individual bare soil patches, for example, the shape of the the rising limb of the hydrograph, when transient dynamics associated with individual patch responses might dominate. Hillslope-scale calibration would be expected to produce better results close to the equilibrium conditions of the whole hillslope.

2.4 Testing the homogeneous calibration approach

One clear limitation of the calibration approach adopted here is that it assumes steady-state, kinematic flow conditions. These assumptions may not be valid during the unsteady conditions that often prevail during individual rainstorms[c1] so we used a coupled Saint Venant equation (SVE) - Richards equations model to explore the effects of unsteady, non-kinematic flow; specifically, we compared the hillslope-scale hydrological predictions made using five different roughness schemes. [c2]The model couples the 2D SVE solver used by Bradford and Katopodes (2001) to the 1D Richards equation solver developed by Celia, Bouloutas, and Zarba (1990) [c3](see supporting information Text S2 for model details, soil parameters, and validation simulations). [c4] To enable intercomparison, we designated Manning's equation with n=0.1 as a 'reference scheme', and calibrated the other four schemes to it, using the homogeneous hillslope approach outlined in Section 3.2. We then assessed the disagreement between predictions made using the calibrated (non-Manning) and reference (Manning) schemes. The roughness schemes tested were the cylinder array, Darcy-Weisbach, transitional and laminar schemes listed in Table 1. We note that although the laminar Poiseuille equation lacks a free parameter, flume studies of laminar flow over natural surfaces have observed α values ranging 6-40 times the Poiseuille coefficient, $\alpha = 3\nu/g$ (Dunkerley, 2001; Pan, Ma, Wainwright, & Shangguan, 2016), presumably due to variations in the bed configuration and inundation depths.

To assess the viability of Equation 13 across a range of scenarios, we chose two representative hillslope gradients ($S_o = 0.01$ and 0.1) and five effective rainfall intensities ($p - K_s = 1, 2, 3, 4, 4.9$ cm/hr; with $p = 5$ cm/hr and $K_s = 0.1$, 1.0, 2.0, 3.0, 4.0 cm/hr), as summarized in Table 2. To avoid unsteady infiltration behavior, we assumed that the soil was initially saturated with $i = K_s$, provided there was sufficient water at the surface to supply this infiltration rate. We used the coupled Saint Venant - Richards equation model to simulate a 30 minute rainstorm for all of the parameter combinations listed in Table 2. For each simulation, the model predicts the two-dimensional overland flow

[c1] *OC*: *Text added.*

[c2] *OC*: ~~We addressed this with a model that~~

[c3] ~~Model details, soil parameters, and validation simulations are presented in supporting information Text S1.~~

[c4] *OC*: ~~We used this coupled Saint Venant equation - Richards equation model to assess the disagreement between hillslope-scale hydrological predictions made using a reference roughness scheme - specifically Manning's equation with $n = 0.1$ - and four other schemes calibrated to this reference condition using the homogeneous hillslope approach outlined in Section 3.2~~

Table 2. Parameters for the SVE model simulations, including both homogeneous and patchy hillslope. Where multiple parameters are listed, the cases were run factorially to explore all parameter combinations. For laminar, transitional, Darcy-Weisbach and cylinder array schemes, α_2 values were obtained with the calibration approach outlined in Section 2.3, using Manning's equation with $n = 0.1$ as the reference scheme for vegetated areas. For bare soil areas in the patchy hillslopes, Manning's equation with $n = 0.03$ was applied for all simulations.

Variable	Symbol	Values
All simulations		
Slope gradient (%)	S_o	1%, 10%
Roughness scheme	m	Laminar, Transitional, Manning, Darcy-Weisbach, Cylinder Array
Domain size	L_x, L_y	50 m × 25 m
Storm duration	t_r	30 minutes
Homogeneous hillslope simulations		
Hydraulic conductivity	K_s	0.1, 1, 2, 3, 4 cm/hr
Rainfall intensity	p	5 cm/hr
Patchy hillslope simulations		
Hydraulic conductivity (vegetated)	K_s	3 cm/hr
Rainfall intensity	p	1.5, 3.0, 4.5 cm/hr
Vegetation fraction	ϕ_V	0.2, 0.5, 0.8
Standard deviation of the spatial kernel	σ	1, 5

depth and velocity, the runoff hydrograph, and a map of the cumulative infiltration depth. Hydrological outcomes were compared between roughness schemes using four error assessment metrics, as described in Section 2.6. [c5]Anticipating that this range of scenarios will produce non-kinematic flow conditions, we assessed (i) the 'kinematic-ness' of the flow (that is, how well the flow fields are described by the kinematic wave approximation), and (ii) whether non-kinematic flow conditions are correlated with larger calibration errors (see supporting information Text S3).

2.5 Testing the calibration approach for patchy hillslopes

To test the calibration method on patchy hillslopes, we generated a variety of synthetic vegetation patterns [c1]on a 50 × 25 m gridded domain, following the approach outlined in Crompton, Sytsma, and Thompson (2019). [c2] We created multiple patterns spanning a range of vegetation fractions (ϕ_V) and patch correlation lengthscales (σ), as detailed in Table 2 [c3]and illustrated in supporting information Figure S1.

[c4]

[c5] *OC*: *Text added.*
[c1] *OC*: *Text added.*
[c2] *OC*: *Text added.*
[c3] *OC*: *Text added.*
[c4] *OC*: ~~on a 50 × 25 m gridded domain consisting of 0.5 × 0.5 m grid cells. To generate the patterns, we drew a random number from a uniform distribution (0,1) for each grid cell. We prescribed a vegetation~~

We parameterized the Saint Venant - Richards equation model by treating all bare soil areas as impermeable, with fixed roughness described by Manning's equation with $n = 0.03$. As in the homogeneous simulations, the reference roughness scheme for all vegetated patches was Manning's equation with $n = 0.1$. For each combination of roughness scheme and hillslope parameters (slope, ϕ_V, and rainfall intensity), we obtained α_2 from Equation 13, using the hillslope-scale q_o for all $p \geq K_s$ cases and the patch-scale q_o for all $p < K_s$ cases. We ran the model for factorial combinations of the rainfall intensities, patterns of vegetation cover, and hillslope gradients listed in Table 2. Illustrative model results from the Saint Venant - Richards equation model are presented in Figure 2, showing a vegetation pattern (panel A), cumulative infiltration depth (panel B) and maximum overland flow velocity (panel C).

As a robustness check [c1], we ran the same simulations with the converse calibration approach, where hillslope-scale calibration was replaced by patch-scale, or vice versa (note that the hillslope-scale approach is not viable where $p(1 - \phi_V) + (p - K_s)\phi_V < 0$). Comparison between the results obtained with patch- and hillslope-scale approaches are included in supporting information [c2]Figures S3-S5, which compare the performance of the patch and hillslope-scale matching approaches. For each rainfall scenario, a larger range of calibration errors is observed for patch-scale matching, which we attribute to our estimation of the 'characteristic' lengthscale as the hillslope-mean bare soil patch length.

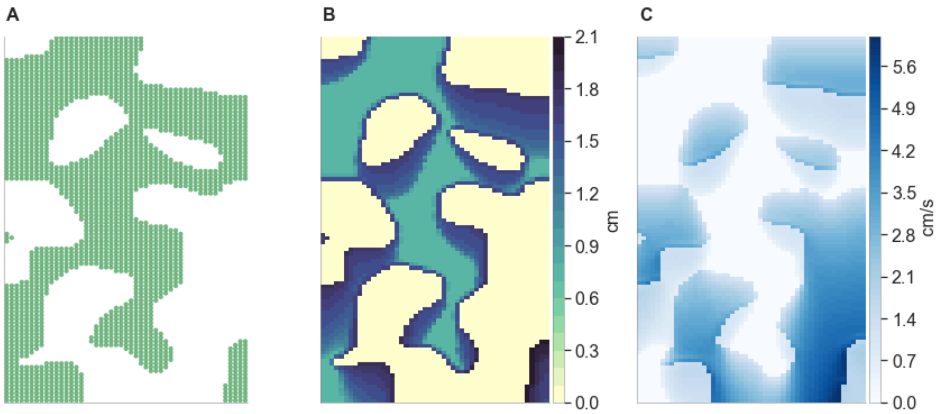

Figure 2. Domain set-up and computed outcomes. (A) map of the spatially random vegetation field with $\phi_V = 0.5$ and $\sigma = 5$ (green circles indicate vegetated 0.5×0.5 m cells). (B) Infiltration map and (C) maximum overland flow velocity resulting from a 30 min duration storm with intensity $p = 1.5$ cm/hour.

fraction as ϕ_V, and classified cells as vegetated (1) or bare (0) around this value. The resulting binary domain was convolved with a symmetrical bivariate Gaussian kernel with standard deviation σ scipy. We again binarized the results around a value selected to preserve ϕ_V. The use of the symmetrical kernel results in isotropic patterns, in which there is no systematic bias in patch properties associated with direction. We created multiple patterns spanning a range of values in ϕ_V and σ, as illustrated in Figure 3 and detailed in Table 3. To provide a more intuitive summary of patch length-scales, we computed the mean, along-slope patch lengths of the vegetated and bare sites, L_v and L_b, obtaining values in the range 2.5-30 m.

[c1] *OC*: on our reasoning in developing the calibration approach for patchy landscapes

[c2] *OC*: Text S3.

2.6 Metrics to evaluate the sensitivity to scheme selection

To assess the sensitivity of hydrological predictions to the choice of a roughness scheme post calibration, we developed four quantitative metrics. For each of these metrics, we computed the difference[c3]s between model simulations [c4]parameterized with the reference scheme (Manning's equation) and [c5]those parameterized with the calibrated schemes.

These metrics were:

1. The hillslope-averaged water balance partitioning, as measured by the infiltration fraction IF, the ratio of the hillslope mean infiltration depth to the rainfall depth.
2. The maximum overland flow velocity, U_{max}.
3. The rising time of the hillslope hydrograph, [c1]t_{rise} estimated as the time at which the hydrograph reached 80% of the maximum discharge obtained from the reference simulation.
4. The hydrograph shape, [c2]computed as a normalized root mean squared error (NRMSE), where the normalizing factor is the maximum discharge from the reference simulation.

[c3]We refer to these differences in hydrological predictions made using different roughness schemes as 'calibration errors'

[c4]

3 Results

3.1 Homogeneous hillslopes

The homogeneous hillslope cases [c5]were used to to assess the effectiveness of the analytical calibration approach in preserving hillslope-scale hydrological behavior [c6](as quantified by the error metrics listed in Section 2.6) across different roughness schemes. [c7]The calibration errors are presented in Figure 3, which summarizes the differences in infiltration fraction IF, hydrograph characteristics, and U_{max} between [c8]the calibrated simulations and the reference Manning's equation simulations.

Numerical instabilities occurred in laminar simulations with $K_s \leq 1.0$ cm/hr, and these simulations were therefore not used in the analysis. [c9]These instabilities are inherent to the numerical scheme used for solution, which does not use additional stabilizing techniques such as adding diffusion (Zarmehi, Tavakoli, & Rahimpour, 2011). There are systematic differences in the errors across roughness schemes: the Darcy-Weisbach and transitional formulations are most similar to the Manning predictions following calibration, and the laminar and cylinder array schemes are most different. This pattern reflects variation in the differences between each conveyance equation's m exponent and

[c3] *Text added.*
[c4] *OC*: ~~using the~~
[c5] *Text added.*
[c1] *OC*: *Text added.*
[c2] *OC*: ~~normalized by the maximum discharge from the reference simulation.~~
[c3] *Text added.*
[c4] *OC*: ~~Differences in univariate metrics between schemes were computed as simple differences, and differences in the hydrographs were computed as a normalized root mean squared error (NRMSE).~~
[c5] *OC*: ~~provide a means~~
[c6] *OC*: *Text added.*
[c7] *OC*: ~~Error metrics measuring differences in this behavior are presented in Figure~~
[c8] *OC*: ~~the calibrated and reference Manning's equation simulations~~
[c9] *OC*: *Text added.*

Manning's equation ($m = 2/3$). These differences are larger for the laminar ($m = 2$) and cylinder array ($m = 0$) schemes than for the Darcy-Weisbach ($m = 1/2$) and transitional ($m = 1$) schemes. However, the practical implications for prediction differences are small: [c10]the standard deviation of the prediction differences is 1.1% for IF, 2.3% for U_{max}, 6.1% for t_{rise} and 3.4% for the hydrograph NRMSE. Hydrograph NRMSE reflect the different shapes of the hydrographs (e.g., Figure 3, Panels E and F), which are unlikely to be important in practical applications. The results suggest that Equation 13 provides [c11]an effective means to parameterize different roughness schemes to represent equivalent flow conditions, allowing for objective inter-comparison [c12]and assessment of the discrepancy between the physics implicit to each roughness scheme.

To estimate the differences in prediction between the most disparate schemes, we also undertook a pairwise comparison between all schemes. We note, however, that all simulations are calibrated to Manning's equation, so this pairwise comparison does not represent the errors that would be generated by direct calibration of the compared schemes to each other. Supporting information Table S4 displays the mean pairwise calibration error for each assessment metric, with the range of values in parentheses. The prediction differences are, unsurprisingly, greatest for the comparison between cylinder array and laminar schemes.

To assess whether the differences in prediction were statistically significant, we used the Wilcoxon signed-rank test of the null hypothesis that the mean difference in predicted hydrological outcomes between two schemes is equal to 0. For each possible pairwise combination of roughness schemes, and for the 4 hydrological assessment metrics, we obtained p-values less than 0.02, and therefore conclude that the sensitivity of the results to the choice of roughness scheme is statistically significant.

3.2 Patchy hillslopes

Differences in predictions between the reference and calibrated simulations for patchy hillslopes reflect errors associated with the adaptation of the homogeneous calibration procedure to patchy hillslopes, in addition to those arising from the calibration procedure itself. Further, on patchy hillslopes, departures from kinematic conditions at patchy boundaries potentially add an additional source of error. The fraction of the hillslope held in common between all cases (the bare sites), however, acts to reduce the magnitude of the differences between cases. The resulting differences between reference and calibrated simulations are shown in Figure 4, which summarizes the differences in IF, U_{max} and hydrograph characteristics for all cases. The hillslope-scale calibration approach was used for the $p = 3.0$ and 4.5 cm/hr rainfall cases, and the patch-scale approach was used for the $p = 1.5$ cm/hr cases. [c5]

The paired simulations show close agreement: [c6]the standard deviation of the prediction differences are 1.1% for IF, 2.3% for U_{max}, 6.0% for the hydrograph NRMSE, and 3.3% for t_{rise}. In absolute units and grouped by scheme, the median U_{max} differences range from -0.3 cm/s (cylinder array) to 0.3 cm/s (laminar), and the median t_{rise} errors range from -0.2 min (cylinder array) to 0.6 min (laminar). The hydrograph

[c10] *OC*: ~~simulations differ by less than 6% for IF and 2% for U_{max} in all cases. The hydrograph rising times differ by less than 9.1% in all cases, and the hydrograph NRMSE are less than 14%.~~

[c11] *OC*: ~~a viable~~

[c12] *OC*: *Text added.*

[c5] *OC*: ~~Numerical instabilities affected the laminar simulations with 20% vegetation cover and $p \geq 3$ cm/hr, and these simulations were excluded from the analysis.~~

[c6] *OC*: ~~the IF differences are less than 4.3%, and the U_{max} differences are less than 7.4% (1.7 cm/hr in absolute units). The differences in t_{rise} are less than 3.4 minutes in all cases. The hydrograph NRMSE are less than 12% across schemes, and less than 4% for the Darcy-Weisbach and transitional schemes~~

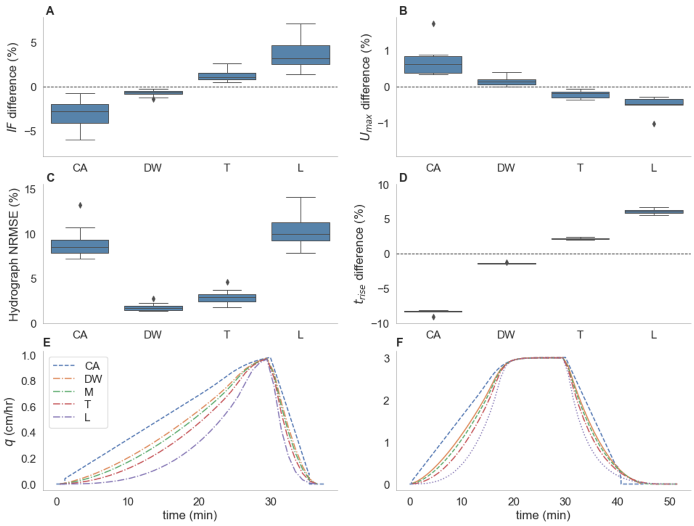

Figure 3. [c3]Box-plots show the differences between each of the non-Manning roughness scheme simulations (cylinder array, CA; Darcy-Weisbach, DW; transitional, T; and laminar, L) and its paired Manning simulation: (A) the infiltration fraction IF, (B) the maximum velocity U_{max}, (C) the hydrograph rising time t_{rise}, and (D) the NRMSE between hydrographs. [c4]Panels (E) and (F) show the simulation hydrographs with the largest NRMSE and differences t_{rise}, respectively : (E) $K_s = 4.0$ cm/hr and $S_o = 0.01$, and (F) $K_s = 2.0$ cm/hr and $S_o = 0.01$.

NRMSE are again larger than the other metrics, due to the differently shaped hydrographs. Overall, these errors are comparable to those produced on homogeneous slopes, and suggests that the additional sources of error in these simulations are compensated for by the use of identical roughness schemes for bare soil sites. The results shown in Figure 4 suggest that the sensitivity of hydrological predictions to the choice of roughness scheme for vegetated surfaces is small, provided the roughness parameters are appropriately calibrated. Similarly to the homogeneous hillslopes, the disagreement between schemes is greatest where the difference between the m exponents in the conveyance equations is largest.

As with the homogeneous hillslopes, we undertook a pairwise comparison between all schemes. Supporting information Table S5 displays the mean pairwise calibration error for each assessment metric, with the range of values in parentheses, again showing the greatest differences between cylinder array and laminar schemes.

We used the Wilcoxon signed-rank test for each of the 4 hydrological metrics and the 10 possible pairwise scheme combinations. We obtained p-values less than 1×1^{-5} for all cases, indicating statistically significant sensitivity of the results to the choice of roughness scheme.

4 Discussion and Conclusions

The results demonstrate the efficacy of a simple kinematic framework to calibrate roughness schemes against each other in order to represent a common flow environment for the case of shallow, rainfall-induced overland flow on natural hillslopes. The key value of the approach is that by imposing kinematic assumptions, calibration can be achieved analytically for both homogeneous or patchily vegetated hillslopes, as demonstrated by comparison of numerical simulations that have been analytically calibrated to represent

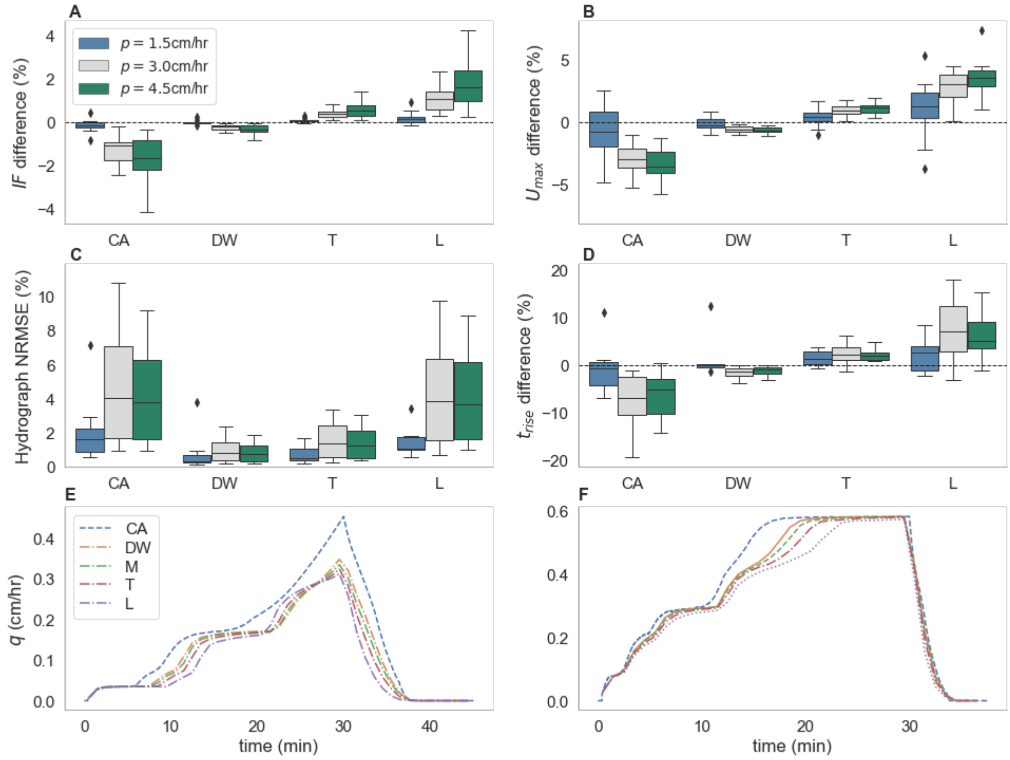

Figure 4. Box-plots show the differences between each of the non-Manning roughness scheme simulations (cylinder array, CA; Darcy-Weisbach, DW; transitional, T; and laminar, L) and its paired Manning simulation: (A) the infiltration fraction IF, (B) the maximum velocity U_{max}, (C) the hydrograph rising time t_{rise}, and (D) the NRMSE between hydrographs.
Panels (E) and (F) show the simulation hydrographs with the largest NRMSE and difference in t_{rise}, respectively.

equivalent flow conditions. The calibrated equations make highly comparable hydrologic predictions for the same hillslope and storm conditions, regardless of the specific roughness schemes selected. This suggests that SVE flow predictions are more sensitive to the value of the roughness coefficient α than to differences in the functional form of the resistance equation, provided the schemes are calibrated to a common flow condition, produced by the same rainfall forcing on the same hillslope. This agreement is likely a consequence of the relatively constrained range of velocity and depth values that arise during rain-induced shallow overland flow. Thus, these results should not be extrapolated to situations with deeper or more variable flow regimes. Similarly, the model results presented here assume that the Saint Venant - Richards equation model adequately represents overland flow dynamics, and that the features of the flow that were omitted - including explicit treatment of emergent roughness elements and microtopography - would not significantly alter the findings. This assumption seems reasonable in light of the agreement between our modeling findings and the experimental results obtained by Cea et al. (2014), who compared high resolution flow simulations with experimental flow data generated on 1×1 m plaster moulds. Like us, they found strong agreement between flow predictions made with different roughness schemes, once those schemes were calibrated.

The hydrological outcomes predicted by the different roughness schemes, as reported in Figures 3 and 4, are not indistinguishable. The differences in predictions, however, are smaller or comparable to measurement uncertainties reported in empirical hydrological studies, including in estimated rainfall rates (e.g. rain gauge under-catch results in systematic under-estimates in the range 5–16%, McMillan, Krueger, & Freer, 2012); in flow velocities (e.g. on the order of 3.0 cm/s using Large Scale Particle Image Velocimetry, Cea et al., 2014, larger than the calibration errors associated with velocities here); and in discharge data (e.g. approximate uncertainty in runoff derived from stage measurements at plot scales range from 10–20%, Krueger et al., 2009; Turnbull, Wainwright, & Brazier, 2010). Thus, the selection of a roughness scheme is unlikely to produce errors that could be readily distinguished from experimental noise. We note that uncertainties associated with field observations are rarely quantified in the literature (Brazier, Krueger, & Wainwright, 2014; Turnbull et al., 2010), precluding a more comprehensive analysis.

This study has presented an analytic approach by which to parameterize different roughness schemes to represent common hillslope surface conditions. We have shown that the kinematic wave approximation provides a suitable framework for calibrating roughness parameters, as evidenced by the close agreement between the various schemes in the simulation results. With a common representation of the surface roughness (via parameterization of α) important hydrological outcomes, including the water balance partitioning, flow velocity and runoff hydrograph, display only minor sensitivity to the selection of a roughness scheme. Consequently, choosing the correct roughness scheme appears less significant than correctly parameterizing any selected scheme. Despite this practical implication, the results here do not assist in determining the correct roughness value for a given scheme. Thus, roughness parameterization remains an open question, subject to ongoing research.

Acknowledgments

This manuscript relied only on model output generated by the authors during the course of the study. OC and SET acknowledge funding from the National Science Foundation (NSF) grant number NSF-EAR-BSF 1632494. GK acknowledges support from NSF-AGS-1644382 and NSF-IOS-1754893. We thank SF Bradford and ND Katopodes for providing the code for the SVE solver described in Bradford and Katopodes (1999), and Tal Svoray and Shmuel Assouline for helpful comments on the draft.

The source code for the SVE model is hosted openly on GitHub:

https://github.com/octavia-crompton/SVE-R. The SVE solver is in Fortran, and Python wrapper scripts are provided to interface with Fortran. Jupyter notebooks are provided to visualize the results for selected examples. Model output is available from the authors on request.

References

Abrahams, A. D., Parsons, A. J., & Wainwright, J. (1994). Resistance to overland flow on semiarid grassland and shrubland hillslopes, walnut gulch, southern arizona. *Journal of Hydrology*, *156*(1-4), 431–446.

Alley, W., & Veenhuis, J. (1983). Effective impervious area in urban runoff modeling. *Journal of Hydraulic Engineering*, *109*(2), 313–319. doi: 10.1061/(ASCE)0733-9429(1983)109:2(313)

Assouline, S. (2004). Rainfall-induced soil surface sealing. *Vadose Zone Journal*, *3*(2), 570–591.

Assouline, S., Thompson, S., Chen, L., Svoray, T., Sela, S., & Katul, G. (2015). The dual role of soil crusts in desertification. *Journal of Geophysical Research: Biogeosciences*, *120*(10), 2108–2119.

Booth, D., & Jackson, C. (1997). Urbanization of aquatic systems: degradation thresholds, stormwater detection, and the limits of mitigation. *JAWRA Jour-*

nal of the American Water Resources Association, *33*(5), 1077–1090. doi: 10.1111/j.1752-1688.1997.tb04126.x

Bracken, L., Cox, N., & Shannon, J. (2008). The relationship between rainfall inputs and flood generation in south–east spain. *Hydrological Processes: An International Journal*, *22*(5), 683–696.

Bradford, S. F., & Katopodes, N. D. (1999). Hydrodynamics of turbid underflows. i: Formulation and numerical analysis. *Journal of Hhydraulic Eengineering*, *125*(10), 1006–1015. doi: 10.1061/(ASCE)0733-9429(1999)125:10(1006)

Bradford, S. F., & Katopodes, N. D. (2001). Finite volume model for nonlevel basin irrigation. *Journal of Iirrigation and Ddrainage Eengineering*, *127*(4), 216–223.

Brazier, R. E., Krueger, T., & Wainwright, J. (2014). Uncertainty assessment. In *Patterns of land degradation in drylands* (pp. 265–285). Springer.

Brutsaert, W. (2005). *Hydrology: Aan iintroduction*. Cambridge University Press.

Cantón, Y., Solé-Benet, A., De Vente, J., Boix-Fayos, C., Calvo-Cases, A., Asensio, C., & Puigdefábregas, J. (2011). A review of runoff generation and soil erosion across scales in semiarid ssouth-eeastern spain. *Journal of Arid Environments*, *75*(12), 1254–1261.

Cea, L., Legout, C., Darboux, F., Esteves, M., & Nord, G. (2014). Experimental validation of a 2d overland flow model using high resolution water depth and velocity data. *Journal of Hhydrology*, *513*, 142–153.

Celia, M. A., Bouloutas, E. T., & Zarba, R. L. (1990). A general mass-conservative numerical solution for the unsaturated flow equation. *Water Rresources Rresearch*, *26*(7), 1483–1496.

Cheng, N.-S., & Nguyen, H. T. (2010). Hydraulic radius for evaluating resistance induced by simulated emergent vegetation in open-channel flows. *Journal of Hydraulic Engineering*, *137*(9), 995–1004.

Crompton, O., Sytsma, A., & Thompson, S. (2019). Emulation of the saint venant equations enables rapid and accurate predictions of infiltration and overland flow velocity on spatially heterogeneous surfaces. *Water Resources Research*.

Descroix, L., Viramontes, D., Estrada, J., Barrios, J.-L. G., & Asseline, J. (2007). Investigating the spatial and temporal boundaries of Hortonian and Hewlettian runoff in Northern Mexico. *Journal of Hhydrology*, *346*(3-4), 144–158.

Dunkerley, D. (2001). Estimating the mean speed of laminar overland flow using dye injection-uncertainty on rough surfaces. *Earth Surface Processes and Landforms*, *26*(4), 363–374.

Dunne, T. (1983). Relation of field studies and modeling in the prediction of storm runoff. *Journal of Hydrology*, *65*(1-3), 25–48.

Gauckler, P. (1867). *Etudes théoriques et pratiques sur l'ecoulement et le mouvement des eaux*. Gauthier-Villars.

Hallema, D. W., Moussa, R., Sun, G., & McNulty, S. G. (2016). Surface storm flow prediction on hillslopes based on topography and hydrologic connectivity. *Ecological Processes*, *5*(1), 13.

Horton, R. E. (1938). The interpretation and application of runoff plot experiments with reference to soil erosion problems. In *Soil science society of america proceedings* (Vol. 3, pp. 340–349).

Jain, M. K., Kothyari, U. C., & Raju, K. G. R. (2004). A gis based distributed rainfall–runoff model. *Journal of Hydrology*, *299*(1-2), 107–135.

Katul, G. G., Poggi, D., & Ridolfi, L. (2011). A flow resistance model for assessing the impact of vegetation on flood routing mechanics. *Water Resources Research*, *47*(8).

Kirstetter, G., Hu, J., Delestre, O., Darboux, F., Lagrée, P.-Y., Popinet, S., ... Josserand, C. (2016). Modeling rain-driven overland flow: Empirical versus analytical friction terms in the shallow water approximation. *Journal of Hydrology*, *536*, 1–9.

Krueger, T., Quinton, J. N., Freer, J., Macleod, C. J., Bilotta, G. S., Brazier, R. E., . . . Haygarth, P. M. (2009). Uncertainties in data and models to describe event dynamics of agricultural sediment and phosphorus transfer. *Journal of Environmental Quality*, *38*(3), 1137–1148.

Lee, J. G., & Heaney, J. (2003). Estimation of urban imperviousness and its impacts on storm water systems. *Journal of Water Resources Planning and Management*, *129*(5), 419–426. doi: 10.1061/(ASCE)0733-9496(2003)129:5(419)

Leopold, L. (1968). Hydrology for urban land planning: a guidebook on the hydrological effects of urban land use. *US Geological Survey*, 18.

Li, H.-Y., Sivapalan, M., Tian, F., & Harman, C. (2014). Functional approach to exploring climatic and landscape controls of runoff generation: 1. behavioral constraints on runoff volume. *Water Resources Research*, *50*(12), 9300–9322.

Lighthill, M. J., & Whitham, G. B. (1955). On kinematic waves ii. a theory of traffic flow on long crowded roads. *Proc. R. Soc. Lond. A*, *229*(1178), 317–345.

Manning, R., Griffith, J. P., Pigot, T., & Vernon-Harcourt, L. F. (1890). *On the flow of water in open channels and pipes.*

McMillan, H., Krueger, T., & Freer, J. (2012). Benchmarking observational uncertainties for hydrology: rainfall, river discharge and water quality. *Hydrological Processes*, *26*(26), 4078–4111.

Mügler, C., Planchon, O., Patin, J., Weill, S., Silvera, N., Richard, P., & Mouche, E. (2011). Comparison of roughness models to simulate overland flow and tracer transport experiments under simulated rainfall at plot scale. *Journal of Hydrology*, *402*(1-2), 25–40.

Pan, C., Ma, L., Wainwright, J., & Shangguan, Z. (2016). Overland flow resistances on varying slope gradients and partitioning on grassed slopes under simulated rainfall. *Water Resources Research*, *52*(4), 2490–2512.

Smith, M. W., Cox, N. J., & Bracken, L. J. (2007). Applying flow resistance equations to overland flows. *Progress in Physical Geography*, *31*(4), 363–387.

Tanino, Y., & Nepf, H. M. (2008). Laboratory investigation of mean drag in a random array of rigid, emergent cylinders. *Journal of Hydraulic Engineering*, *134*(1), 34–41.

Thompson, S., Harman, C., Heine, P., & Katul, G. (2010). Vegetation-infiltration relationships across climatic and soil type gradients. *Journal of Geophysical Research: Biogeosciences*, *115*(G2).

Turnbull, L., Wainwright, J., & Brazier, R. E. (2010). Changes in hydrology and erosion over a transition from grassland to shrubland. *Hydrological Processes: An International Journal*, *24*(4), 393–414.

Wang, W.-J., Huai, W.-X., Thompson, S., & Katul, G. G. (2015). Steady nonuniform shallow flow within emergent vegetation. *Water Resources Research*, *51*(12), 10047–10064.

Zarmehi, F., Tavakoli, A., & Rahimpour, M. (2011). On numerical stabilization in the solution of saint-venant equations using the finite element method. *Computers & Mathematics with Applications*, *62*(4), 1957–1968.